X-ray-absorption fine-structure standards: A comparison of experiment and theory

G. G. Li, F. Bridges, and C. H. Booth

Physics Department, University of California, Santa Cruz, California 95064

(Received 24 October 1994)

The reliability of the structural parameters obtained from x-ray-absorption fine-structure (XAFS) spectra strongly depends on the quality of the standards used in the data analyses. We have compared about 30 isolated pair standards, extracted from experimental data, with those generated by the FEFF5 code. The absorbing atoms range from Ni ($Z=28$) to Pb ($Z=82$) and the backscattering atoms from O ($Z=8$) to Au ($Z=79$). In general, good agreement is achieved, with typical errors of 0.005 Å for nearest-neighbor distances R. Significant differences are sometimes found in the backscattering amplitude $F(k, R)$ at low values of the photoelectron wave vector k (< 7 Å^{-1}), especially for heavy backscattering atoms such as Au and Pt. We demonstrate that when there are significant differences between experimental and theoretical functions, $F(k, R)$, an experimental standard, shifted from one atom pair to another, provides a better fit to the data than obtained using the theoretical standard and reduces the errors in amplitude and position, often by a factor of 2–3. The effective amplitude reduction factor $S_{o,\text{eff}}^2$ and the E_o shift for the calculated XAFS standards are also given; the former can vary by $\pm$ 20% across the Periodic Table. Estimated experimental errors for the amplitudes are $< 10\%$, and $\sim$5–6 % in many cases. Some important fundamental issues, such as background removal, the influence of the energy resolution on XAFS, and correlations in the fitting parameters, are also addressed.

I. INTRODUCTION

The x-ray-absorption fine-structure (XAFS) technique[1,2] utilizes the interference effect between the outgoing photoelectron wave, produced when an x ray is absorbed by an atom, and the fraction of this wave that is backscattered from neighboring atoms. Thus XAFS contains information about the distances to and the number of neighboring atoms, from the point of view of a central absorbing atomic species (selected by scanning over the appropriate x-ray energy). It can therefore determine the average local structure of different elements independently. The combination of information from different types of absorbing atoms can give a more constrained result for the *local* structure than diffraction experiments. Furthermore, since XAFS analysis does not make use of long-range translational symmetry, local deviations of atoms from the symmetry positions are easier to identify. Consequently, the XAFS technique has been widely recognized and utilized as a tool for local structural studies, especially in systems lacking long-range order, such as systems with defects and local distortions, where traditional diffraction studies can only provide information about the average structure.

XAFS data analyses are usually carried out using a least-squares fitting procedure in which the data is fit to a sum of XAFS atom-pair standards.[1,2] Each standard has three main parameters—the amplitude (number of neighbors), the atom-pair distance, and the Debye-Waller-like broadening parameter. These parameters, particularly the number of neighbors and positions of the backscattering atoms, determine the local structure. Consequently, the quality of the XAFS structural results strongly depends on the quality of the XAFS standards used in the data analyses. Two types of XAFS standards are commonly used, experimental standards and theoretical standards. The former are extracted from XAFS data, collected at low temperatures, for model compounds with relatively simple crystal structures. When the atom pair in the model compound and in the real sample have reasonably similar chemical environments, the experimental standard for that atom pair usually works very well. However, an appropriate model compound is not always available. For these cases, the theoretical XAFS standards are desirable. A number of theoretical calculations have been carried out over the past 15 years[3–10] and the quality of the theoretical XAFS standards has improved dramatically. One of the recent codes, FEFF (Refs. 7–10) (we use FEFF5 and FEFF6), developed by Rehr and co-authors, gives good agreement to the experimental data and has been widely used in XAFS data analyses. It has been demonstrated for a few samples[7,8] that the calculated XAFS are typically accurate to within 15% in amplitude and 0.02 Å in distance for the nearest neighbors.

In this paper we show that theoretical XAFS standards, calculated using the FEFF5 (or FEFF6) code, are in many cases better [in terms of the shape of $F(k, R)$ and the bond length] than previously expected. Using known standards, the amplitude of the calculated XAFS can be calibrated (i.e., the amplitude reduction factor, S_o^2, determined) to minimize the error in the extracted number of neighboring atoms in unknown samples. However, we find in a few cases, especially at high Z, that the experimental standards are still much better than the theoretical ones. Preliminary results were reported

earlier.[11]

We begin in Sec. II, with a brief description of the XAFS measurements, followed, in Sec. III, by a discussion of the background removal procedure and data analysis methods. The extraction of the experimental XAFS standards is illustrated in Sec. IV. The main body of the paper, Sec. V, provides detailed comparisons of the experimental and theoretical standards, with subsections on energy resolution effects, the effective amplitude reduction factor $S_{o,eff}^2$, amplitude and phase functions, transferability of experimental standards, and the uncertainties of (and correlations between) the extracted parameters. Here we also address and discuss some fundamental problems in the reduction of XAFS data and its analysis. The results are summarized in Sec. VI.

II. X-RAY-ABSORPTION MEASUREMENTS

The XAFS data were collected at the Stanford Synchrotron Radiation Laboratory (SSRL) during the past 10 years, using liquid nitrogen or helium cryostats. Si(111), Si(220), and Si(400) double crystal monochromators were used for various absorption edges. For each of the measurements, the double monochromator was detuned to approximately one-half of maximum transmitted x-ray intensity to reduce the harmonic content of the beam. All the data were taken in the transmission mode. The incident and transmitted x-ray intensities were measured using gas ionization chambers, with nitrogen, argon, or krypton gas, depending on the x-ray energy.

For many single element model materials, thin foils were used, with thicknesses in the range 1–3 absorption lengths. Although the thickness was sometimes larger than one absorption length, it did not affect the quality of the XAFS data because the foils were quite uniform and free of pinholes. For compounds, the samples were ground into fine powders, passed through a 30 μm sieve, and brushed onto Scotch tape as uniformly as possible. This process preferentially collects the smaller particles and the average size is well below 30 μm. Between 4 and 20 layers of tape were stacked together to give a step height of roughly one absorption length at the edge of interest. With samples carefully prepared in this way, the influence of the particle size and pinholes (or thickness effect) on the amplitude of the measured XAFS function is expected to be negligible[12,13] and we get consistent results for samples of different thicknesses. The high spatial uniformity also minimizes glitches.[14] Examples of the high signal-to-noise k space data are shown in Fig. 1 for five samples with backscattering atoms in the second to the sixth row of the Periodic Table.

For a powder sample, the particles in the sample may not be totally randomly oriented due to the anisotropic shape of the particles for noncubic materials; this is often called the texture effect.[15] This effect is weak when the particle-size is small. In this study, almost all the compounds have either cubic or hexagonal close-packed structures. The only exceptions are CuO, which is monoclinic with $a = 4.68$ Å, $b = 3.42$ Å, $c = 5.13$ Å, and $\gamma = 99.54°$, and β-PbO$_2$, which is tetragonal with $a = 4.955$
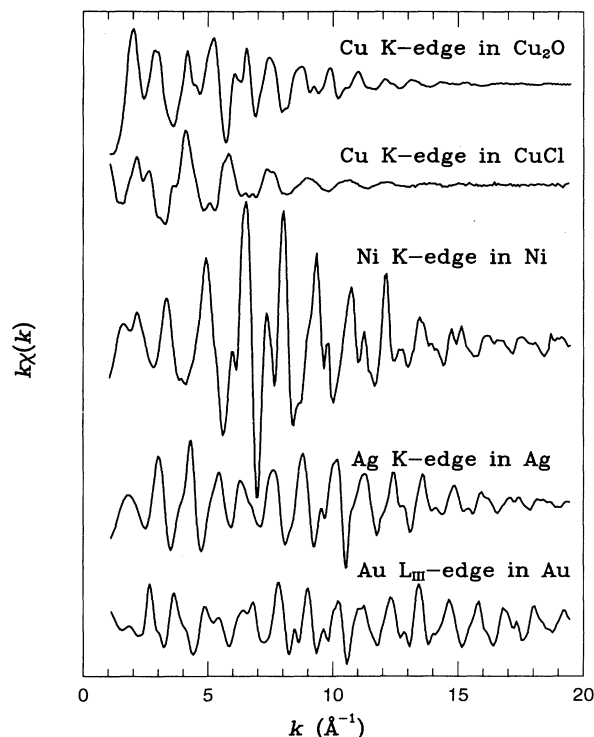

FIG. 1. XAFS function, $k\chi(k)$, collected at the Cu K edge in Cu$_2$O and CuCl powders, Ni K edge in Ni foil, Ag K edge in Ag foil, and the Au L_{III} edge for Au foil.

and $c = 3.383$. Samples with these structures should have little or no preferred orientation of grains.

III. BACKGROUND REMOVAL AND DATA ANALYSIS

The XAFS function, $\chi(E)$, is obtained using the equation $\chi(E) = [\mu(E) - \mu_0(E)]/\mu_0(E)$, where the absorption coefficient $\mu(E)$ includes the absorption from the edge of interest and the XAFS oscillations. $\mu_0(E)$, which we call the "embedded-atom" absorption, is the part of $\mu(E)$ which does not include the XAFS. The main feature in $\mu_0(E)$, i.e., the edge, is due primarily to the absorbing atom. However, many-body effects can cause features in $\mu_0(E)$ which are not present in one electron calculations of an isolated (free) atom's absorption.

Next, $\chi(E)$ is converted to k space, using $k = [2m(E - E_0)]^{1/2}/\hbar$. In order to obtain the function $\chi(k)$, contributions to the absorption from other edges, plus the absorption of other material in the optical path (dewar windows, air, etc.) must be removed. A polynomial fit to the pre-edge data is subtracted from the entire data set[2] to give the absorption for the edge of interest, $\mu(E)$. The polynomial is adjusted at higher energies so that the absorption above the edge, after the pre-edge background removal, follows the Victoreen formula. A careful subtraction is important for obtaining consistent Debye-Waller factors (σ) and amplitudes.

An appropriate embedded-atom absorption coefficient

$\mu_o(E)$ must then be determined. $\mu_o(E)$ is usually approximated by a set of splines or a polynomial function fit to the data using a least-squares algorithm. This approach is based on two assumptions: (1) $\mu_o(E)$ is a smooth function, without any sharp steps or oscillations; (2) the average or weighted average of the XAFS function $\chi(k)$ over a certain k or E region is zero. Very often, it is not straightforward to isolate a smooth background function from the XAFS oscillations in the low-k region. Structure in the background that is not removed will distort the XAFS function. Therefore, the background function has to be carefully determined in order to obtain undistorted (or nearly undistorted) XAFS spectra. Several methods have been proposed in the recent literature.[16-19]

In our data reduction procedure, $\mu_o(E)$ is initially modeled by fitting to a set of splines; each cubic spline is a function of $(E - E_o)^n$, where E_o is defined as the energy at one-half of the absorption edge height and n is usually chosen to be in the range $0.5 \sim 1.0$. The number of spline knots is chosen to remove the background adequately but not to reduce the XAFS amplitude significantly. The high end of the fitting range, E_{max}, is fixed at some point based on the signal-to-noise ratio. The low end of the fitting range, E_{min}, is an adjustable parameter which usually ranges from 5 to 30 eV above E_o. Our criterion for choosing E_{min} is to obtain a monotonic and smooth amplitude function in the Fourier transformed (r space) data at small r.

Several methods have been implemented in our code to automate the determination of E_{min} over a certain energy range. E_{min} is varied to minimize either (i) the area under the amplitude function in the low-r region below the first peak, typically over the range 0–1 Å or (ii) the difference between the amplitude function and a quadratic function in the low-r side of the first peak. The latter suppresses oscillations in the amplitude function and tends to make the amplitude decrease monotonically with r as r goes to zero. The first method is usually used when the position of the first peak is higher than 2 Å, while the second method is commonly used when the first peak is below 2 Å. This automated procedure works very well in most cases.

When well defined steps or oscillations show up in the background and/or a non-XAFS low-r peak or hump in the r space data cannot be removed easily by the above method, an iterative background removal method[16,20] is used. We first use a set of splines to obtain a rough estimate of the background and fit the extracted XAFS data to a sum of theoretical standards. The resulting fit parameters are used to generate an XAFS function over a wide range in k space for the first few neighbors. This function is converted to an E space function and then subtracted from the raw data in E space yielding a residue function. The residue function is then fit to splines as before to obtain a better background, $\mu_o(E)$, which is used to re-reduce the raw data. The process converges in a few iterations. This technique enables us to extract the XAFS function correctly[21,22] and to study the embedded-atom absorption features in the XAFS region.[16,23] Several examples of the background functions used in this study are shown in Fig. 2. The

steps and oscillations in the extracted background are from multielectron excitations (see Refs. 16 and 24 and references therein) and possibly "atomic XAFS,"[23] and typically have amplitudes from 0.5 to 3% of the edge height. These structures need to be removed in a careful XAFS analysis. However, multielectron excitations and atomic XAFS are also of interest; we intend to address the background features in Fig. 2 in a future paper.

Once the proper background has been determined, the XAFS function $\chi(k)$ can be obtained. This function can be decomposed in the following way:

$$k\chi(k) = \sum_j N_j A_j(k, R_j) \int \frac{\sin[2kr + P_j(k)]}{r^2} \frac{1}{\sigma\sqrt{2\pi}}$$
$$\times \exp\left[-\frac{(r - R_j)^2}{2\sigma^2}\right] dr, \qquad (1)$$

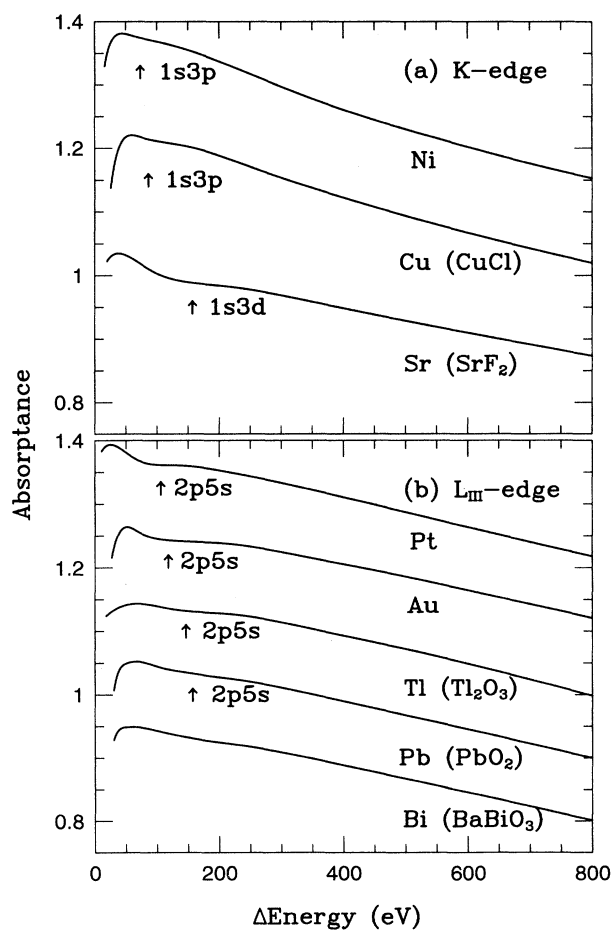where the sum is taken over shells with N_j atoms

FIG. 2. Some examples of the XAFS background functions for the Ni, Cu, and Sr K edges and the Pt, Au, Tl, Pb, and Bi L_{III} edges, extracted from the (low-temperature) experimental data using the iterative background extraction method.[16,20] The functions have been normalized to one at the edge and the functions are vertically displaced for presentation. The positions of some possible multielectron excitations, obtained from the "$Z+1$" model, are indicated.

at a distance R_j from the absorbing atom. Here $A_j(k, R_j)$ is the amplitude function; $A_j(k, R_j) = S_o^2 F_j(k, R_j) \exp[-2R_j/\lambda(k)]$, where $F_j(k, R_j)$ is the backscattering amplitude, $\lambda(k)$ is the effective electron mean-free path, and S_o^2 is the amplitude correction factor. $P_j(k)$ is the phase function, $P_j(k) = 2\delta_c(k) + \phi_j(k)$, where $\delta_c(k)$ is the central-atom phase shift and $\phi_j(k)$ is the backscattering-atom phase shift. A Gaussian distribution function, $\frac{1}{\sigma\sqrt{2\pi}} \exp[-\frac{(r-R_j)^2}{2\sigma^2}]$, is usually used as a pair distribution function, where σ_j^2 is the mean-square fluctuation of R_j. Finally, the experimental data $k^n \chi(k)_{\mathrm{exp}}$ are Fourier transformed (FT) into real (r) space; we define this function as $\tilde{\chi}_{\mathrm{exp}}^n(r)$, where $n=1$ for most of this paper. To obtain numerical values for R_j, N_j, and σ_j, we perform iterated least-square fits to the real $(\mathrm{Re}[\tilde{\chi}_{\mathrm{exp}}^1(r_i)])$ and imaginary $(\mathrm{Im}[\tilde{\chi}_{\mathrm{exp}}^1(r_i)])$ parts of the FT of $k\chi(k)_{\mathrm{exp}}$ using identically k space transformed standards $[\tilde{\chi}_{\mathrm{std}}^1(r_i)]$. In these fits, the overlaps of the radial distributions of neighbors in r space are included. The quality of fit parameter, C^2, with uniform weighting is given by

$$C^2 = \sum_i^N \left(\frac{[\mathrm{Re}(\tilde{\chi}_{\mathrm{exp}}^1(r_i) - \tilde{\chi}_{\mathrm{std}}^1(r_i))]^2}{\sum_j [\mathrm{Re}(\tilde{\chi}_{\mathrm{exp}}^1(r_j))]^2} \right.$$
$$\left. + \frac{[\mathrm{Im}(\tilde{\chi}_{\mathrm{exp}}^1(r_i) - \tilde{\chi}_{\mathrm{std}}^1(r_i))]^2}{\sum_j [\mathrm{Im}(\tilde{\chi}_{\mathrm{exp}}^1(r_j))]^2} \right), \qquad (2)$$

where the sum is over all N points in the range of the structural feature being fit.

Assuming that the noise distribution in r space is flat within the fitting range, Eq. (2) is proportional to a fractional χ-square — $\sqrt{C^2}$ is the average fractional error per point. However, XAFS data analysis is somewhat different than analyses in other experiments such as x-ray photoemission spectroscopy and diffraction, in that a sum of XAFS standards (generated either theoretically or experimentally) are used in the fit. These standards are complicated functions, not a sum of simple universal functions such as Gaussians or Lorentzians, and have systematic errors. Thus the C^2 value usually depends on the r space fitting range, the k space FT range, and the particular standards used. In many cases we have found that for high S/N data, the largest errors arise in the standards. Consequently it is impossible to estimate the correct uncertainty to put into the standard equation for a χ-squared fit. It is very important, both in reducing the data and in generating the appropriate standards, that the shape of either the data or the standard function $\chi(k)$ not be distorted. Otherwise C^2 cannot be reduced below some value determined by the distortions. This will be discussed in more detail in Sec. V F.

IV. GENERATING
AN EXPERIMENTAL STANDARD

We take the Au-Au pair as an example to show the extraction procedure for an experimental XAFS standard. After removing the background, the reduced XAFS data, $k\chi(k)$, are Fourier transformed to r space, using as long a k space interval as possible. Second, the data are fit, using a sum of transformed theoretical standards, within a fixed range in r space. For the case of Au, the data were fit over the range of 1.8~5.8 Å; four pairs were included in the fit at $r=2.88$ Å, 4.07 Å, 4.98 Å, and 5.75 Å, respectively. Those standards were calculated using FEFF5 and an 8 Å-radius-Au cluster with the absorbing atom located at the center. For the more distant neighbors, several multiple-scattering contributions were lumped together with the single scattering pair which had nearly the same effective path length, and the whole function was treated as an ordinary single scattering pair. These standards fit the data very well as shown in Fig. 3(a). A small but significant difference in the shape of the first neighbor peak near 2.7 Å is observed and can be greatly minimized by introducing a constant phase shift which will be discussed in Sec. V D. The extracted structural parameters for Au obtained in this fit are in excellent agreement with the diffraction results, as shown in Table I. The difference between the fit to Au and diffraction is -0.005 ± 0.002 Å in distance, and 10% in the number of neighboring atoms (with $S_{o,\mathrm{eff}}^2 = 0.86$).

Next the fits to the further shells are subtracted in r space to obtain an isolated first shell standard [Fig. 3(b)], using the fitting parameters obtained above. Finally, this
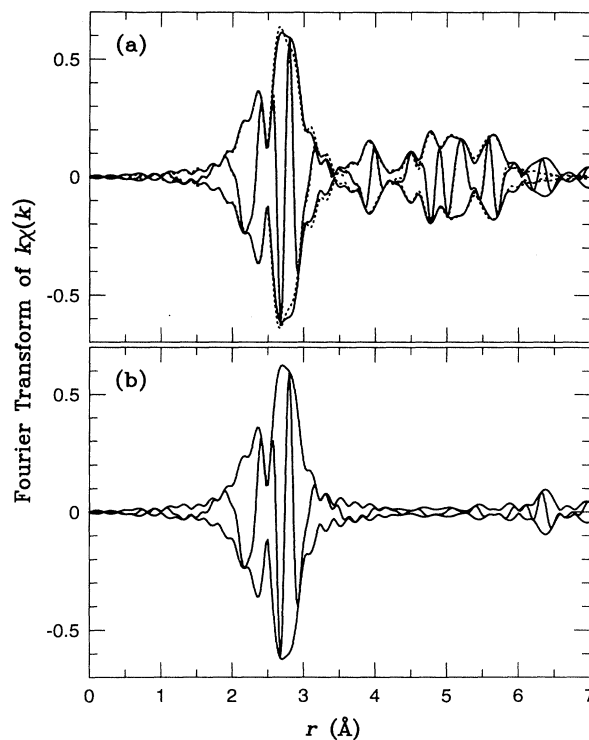

FIG. 3. Generation of an isolated Au-Au experimental pair from the experimental data for Au. (a) Shows the fits (dotted lines) of the sum of theoretical standards to the experimental data (solid lines). (b) The isolated Au-Au experimental pair, with the further shells subtracted off. Fourier transform windows are from 3.5 to 18.5 Å^{-1}, Gaussian rounded by 0.3 Å^{-1}. Both the magnitude and the real part of the transform are plotted.

isolated peak is Fourier transformed back to k space to generate a standard pair (with both real and imaginary parts). The transform range is carefully chosen so that essentially the entire peak is included (ideally from an analysis viewpoint, the magnitude function goes to zero on both sides of the transform limit) but most of the residuals from other shells are excluded. The back-FT standard can be further decomposed[25] into amplitude, $A(k)$ (excluding the N/R^2 factor), and phase, $P(k)$, functions,

$$A(k) = 2\frac{R^2}{N} \sqrt{[\mathrm{Re}(k\chi(k))]^2 + [\mathrm{Im}(k\chi(k))]^2}, \quad (3)$$

$$P(k) = \tan^{-1}\left[\frac{\mathrm{Re}(k\chi(k))}{-\mathrm{Im}(k\chi(k))}\right] - 2kR. \quad (4)$$

These functions can be used to shift the standard for a pair from one distance to another and more importantly

TABLE I. Comparisons of the structural parameters for Ni, Au, NiO, and Cu_2O obtained from diffraction (Diff) and XAFS studies. R (in Å) is the distance to the backscattering atoms, N is the number of neighboring atoms at that distance, and σ (in 10^{-2} Å) is the Debye-Waller factor for the corresponding pair. The values of σ calculated from FEFF5 are noted.

	Shell	1st	2nd	3rd	4th
	Ni [T=83 K, $S_{o,\mathrm{eff}}^2$=0.82, $\Delta t\mu(E_o)$=2.7]				
R	Diff	2.4863	3.5161	4.3063	4.9725
	XAFS	2.482	3.512	4.312	4.976
N	Diff	12.0	6.0	24.0	12.0
	XAFS	12.0	5.4	24.9	15.3
σ	Debye[a] (FEFF5)	5.04	5.47	5.45	5.42
	XAFS	4.8	5.6	6.1	6.6
	Au [T=77 K, $S_{o,\mathrm{eff}}^2$=0.86, $\Delta t\mu(E_o)$=1.1]				
R	Diff	2.8757	4.0669	4.9809	5.7515
	XAFS	2.877	4.065	4.983	5.753
	XAFS[b]	2.876	4.070	4.987	5.757
N	Diff	12.0	6.0	24.0	12.0
	XAFS	12.0	6.6	24.9	13.1
σ	Debye[c] (FEFF5)	5.59	6.16	6.21	6.25
	XAFS	4.7	6.2	6.2	6.4
	NiO [T=83 K, $S_{o,\mathrm{eff}}^2$=1.04, $\Delta t\mu(E_o)$=1.1]				
R	Diff	2.0852	2.949		
	XAFS	2.090	2.951		
N	Diff	6.0	12.0		
	XAFS	6.0	12.6		
σ	Debye[d] (FEFF5)	6.78	4.79		
	XAFS	7.2	6.3		
	Cu_2O [T=83 K, $S_{o,\mathrm{eff}}^2$=0.69, $\Delta t\mu(E_o)$=0.6]				
R	Diff	1.8472	3.0165	3.5372	
	XAFS	1.832	3.015	3.534	
N	Diff	2.0	12.0	6.0	
	XAFS	1.9	12.3	6.3	
σ	XAFS	3.5	8.4	6.2	

[a]Θ_D =450 K, from Ref. 30.
[b]Phase shift=-0.25 rad.
[c]Θ_D =165 K, from Ref. 30.
[d]Θ_D =560 K, from Ref. 31.

they can be used to modify the experimental standard for one pair of atoms to that for another pair of atoms. Examples will be given in Sec. V E. These functions are also very useful for the following detailed comparisons of the experimental and theoretical standards.

V. DETAILED COMPARISONS OF EXPERIMENTAL AND THEORETICAL STANDARDS

A. Overview

Simple and well defined compounds have been chosen to generate the experimental XAFS standards. In this paper we consider 27 experimental standards that we have extracted over the past few years, and compare them with theoretical functions. First, an overall comparison between diffraction and XAFS results was made for the first few shells for each compound. Typical results are listed in Table I for several compounds. The distances to the neighboring atoms are in excellent agreement for all the shells given, with a typical error of 0.005 Å. Using the effective amplitude correction factor, $S_{o,\mathrm{eff}}^2$ described below (see Table II), the agreement in the coordinate number for the further shells in Table I is also excellent, with a typical error $\lesssim 10\%$.

The S_o^2 factor was originally introduced as an amplitude reduction factor, to take into account the influence of many-body effects (such as shake-up and shake-off) on the amplitude of the measured XAFS spectra.[26] Atomic values of S_o^2 have been previously calculated for a photoemission study.[27] Since the outer-shell electrons must play a role in multielectron effects, S_o^2 could vary with chemical environment. Furthermore, errors in the calculation of the core-hole lifetime and other inelastic energy losses which determine the effective mean-free path of the photoelectron, will also strongly affect the measured reduction factors, since the theoretical standards include the "mean-free path" term, $\exp[-2R_j/\lambda(k)]$. All of these effects are included in the experimental value of $S_{o,\mathrm{eff}}^2$; thus in practice we use $S_{o,\mathrm{eff}}^2$ as a total correction factor for the theoretical XAFS amplitude.

We have made detailed comparisons for the 27 isolated atom pairs, listed in Table II. The quality of the fit of the theoretical standards to experimental ones can be seen in the examples shown in Figs. 4–6. These atom-pair standards are generated from the first shell of various model compounds with the further shells subtracted as described in Sec. IV. The distances to the nearest-neighbor atoms, determined by diffraction measurements at room temperature with (sometimes roughly estimated) thermal contraction corrections, are given in the third column of Table II as R_d, the "true" distance. The errors in these distances, obtained from diffraction, are expected to be less than 0.001 Å. The atom-pair distance is often the most important parameter in the XAFS data analysis. Our extensive comparisons show that the agreement in distance between experimental and theoretical standards for the nearest neighbor is usually better than 0.01 Å; in many cases, the agreement is better than

0.005 Å. We have also carried out fits using different k weightings — $k\chi(k)$, $k^2\chi(k)$, and $k^3\chi(k)$. Different k weightings effectively change the region of k space that is emphasized in the fit; in these comparisons however, the extracted atom-pair distance from our fits is essentially independent of the k-space weighting.

The number of neighboring atoms, N, for a given atom pair is another important parameter in XAFS studies. In order to obtain this parameter (and the Debye-Waller factor, σ) correctly when theoretical standards are used, it is necessary to calibrate the amplitude of the theoretical XAFS function via the amplitude correction fac-

TABLE II. Comparisons of experimental and theoretical XAFS standards. R_d is the distance to the nearest neighbor given by diffraction measurements. $\Delta\mu(E_o)t$ is the edge height in the experimental data. The fitting parameters obtained using the theoretical XAFS standards (FEFF5) are given; σ is the Debye-Waller factor; ΔR is the shift in distance relative to R_d; ΔE_o is the shift of the absorption edge relative to the experimentally defined one; $S^2_{o,eff}$ is the amplitude correction factor for the theoretical XAFS standard. The values of $S^2_{o,eff}$ in parentheses are obtained with σ fixed at the indicated theoretical value. Note: variation ranges are estimated using different k weighting [$k\chi(k)$, $k^2\chi(k)$, and $k^3\chi(k)$] in the fits. Actual estimated uncertainties in ΔR are generally < 0.01 Å, and in σ and $S^2_{o,eff}$ are generally < 10%.

Edge	Pair	Compound	R_d(Å)	$\sigma(10^{-2}$ Å)	$\Delta R(10^{-2}$ Å)	ΔE_o(eV)	$S^2_{o,eff}$	$\Delta\mu(E_o)t$	Crystal
Ni (Z=28) K	Ni-O	NiO (83 K)	2.085[a]	6.33±0.47	−0.1±0.1	−2.4±0.1	1.04±0.04	1.1	Si(400)
	Ni-Ni	Ni (83 K)	2.486[b]	4.83±0.01 (5.04)[c]	−0.4±0.1	−0.5±0.2	0.82±0.00 (0.85±0.01)	2.7	Si(220)
Cu (Z=29) K	Cu-O	CuO (83 K)	1.955	4.87±0.12	0.0±0.4	−6.1±0.5	0.64±0.01[d]	1.6	Si(111)
	Cu-O	Cu$_2$O (83 K)	1.847[e]	3.95±0.39	−0.8±0.7	−6.8±1.0	0.69±0.02[d]	0.6	Si(111)
	Cu-Cl	CuCl (4.2 K)	2.342[f]	6.15±0.26	0.0±0.2	−5.2±0.3	0.74±0.02	1.4	Si(111)
	Cu-Cu	Cu (83 K)	2.548[b]	5.56±0.01 (5.75)[c]	−0.4±0.2	0.2±0.3	0.84±0.01 (0.89±0.01)	3.0	Si(220)
	Cu-Br	CuBr (83 K)	2.458[f]	6.45±0.10	−0.5±0.4	−2.5±0.7	0.84±0.02	1.0	Si(220)
	Cu-I	CuI (4.2 K)	2.611[f]	4.61±0.11	−0.9±0.0	−2.5±0.1	0.75±0.01	0.8	Si(111)
Zn (Z=30) K	Zn-Tf	ZnTe (83 K)	2.637[f]	4.50±0.07	0.0±0.3	−4.4±0.7	0.80±0.02	0.7	Si(220)
Br (Z=35) K	Br-Cu	CuBr (83 K)	2.458[f]	6.43±0.02	−0.9±0.0	−3.1±0.2	0.93±0.03	0.6	Si(220)
	Br-Rb	RbBr (83 K)	3.405[g]	8.76±0.09	0.9±0.7	−0.5±1.0	0.94±0.02	0.8	Si(220)
Rb (Z=37) K	Rb-Br	RbBr (83 K)	3.405[g]	9.12±0.18	1.6±0.5	−3.5±0.7	1.2±0.1	0.8	Si(220)
Sr (Z=38) K	Sr-F	SrF$_2$ (4.2 K)	2.499[h]	6.70±0.54	−1.0±0.6	−0.8±0.6	1.13±0.07	0.6	Si(111)
Zr (Z=40) K	Zr-Zr	α-Zr (83 K)	3.202[b]	5.63±0.18 (5.26)[c]	2.0±0.1	−1.3±0.1	1.06±0.05 (0.94±0.01)	0.7	Si(220)
Nb (Z=41) K	Nb-Nb	Nb (83 K)	2.854[b]	5.24±0.04 (5.47)[c]	0.0±0.1	0.1±0.2	1.04±0.01 (1.10±0.02)	0.7	Si(220)
Ag (Z=47) K	Ag-Ag	Ag (83 K)	2.879[b]	5.73±0.05 (6.00)[c]	−0.3±0.3	−3.6±0.9	0.96±0.02 (1.07±0.03)	1.7	Si(220)
	Ag-I	β-AgI (83 K)	2.806[f]	5.74±0.13	0.3±0.5	−4.3±1.2	0.79±0.03	1.7	Si(220)
Cd (Z=48) K	Cd-Cd	Cd (83 K)	2.969[b]	6.17±0.05 (6.11)[c]	0.6±0.1	5.0±0.2	0.97±0.02 (0.96±0.01)	1.1	Si(220)
	Cd-Te	CdTe (83 K)	2.804[f]	4.72±0.09	1.0±0.2	−12.6±0.3	1.01±0.03	1.0	Si(220)
In (Z=49) K	In-Sb	InSb (83 K)	2.803[f]	4.36±0.03	−0.1±0.2	−6.4±0.6	1.04±0.01	1.7	Si(220)
Sn (Z=50) K	Sn-Nb	Nb$_3$Sn (83 K)	2.954[i]	4.95±0.05	0.2±0.0	−4.8±0.1	1.04±0.01	0.8	Si(220)
Sb (Z=51) K	Sb-Nb	Nb$_3$Sb (83 K)	2.939[i]	4.74±0.12	0.2±0.3	−8.5±0.9	1.01±0.03	0.4	Si(220)
Ce (Z=58) K	Ce-O	CeO$_2$ (83 K)	2.340[j]	5.21±0.14	0.2±0.1	3.6±0.1	0.84±0.02	0.8	Si(400)
Pt (Z=78) L_{III}	Pt-Pt	Pt (83 K)	2.77[b]	3.78±0.11 (4.23)[c]	−0.4±0.1	−10.9±0.5	0.88±0.03 (1.01±0.04)	1.1	Si(220)
Au (Z=79) L_{III}	Au-Au	Au (77 K)	2.876[b]	4.93±0.07 (5.59)[c]	−0.5±0.2	−7.6±0.7	0.86±0.02 (1.11±0.01)	1.1	Si(220)
Hg (Z=80) L_{III}	Hg-Te	HgTe (83 K)	2.7955[f]	4.87±0.08	−0.3±0.0	−3.8±0.0	0.75±0.02	0.5	Si(220)
Pb (Z=82) L_{III}	Pb-O	β-PbO$_2$ (83 K)	2.161[j]	5.13±0.11	−0.3±0.2	−1.4±0.4	0.73±0.01	0.6	Si(220)

[a]From Ref. 32.

[b]Calculated from Wyckoff (Ref. 33) with thermal expansion corrections (Ref. 34).

[c]Calculated from FEFF5 with the correlated Debye model. The Debye temperatures are from Ref. 30.

[d]L. Tröger et al. (Ref. 34) measured S^2_o at the O-K edge for CuO and Cu$_2$O to be 0.70 ± 0.05 and 0.63 ± 0.04, respectively.

[e]From Ref. 35.

[f]From Ref. 36.

[g]From Ref. 37. Including a third cumulant gives results consistent with Frenkel et al. (Ref. 19) and does not alter our fit results within the estimated error range.

[h]Extrapolated using the data for 28–284 °C from Ref. 38.

[i]From Ref. 39. The lattice constant of Nb$_3$Sb is corrected using data for Nb$_3$Sn.

[j]Calculated from Wyckoff (Ref. 33) and corrected by the thermal expansion, $\epsilon = (L_{80} - L_{298})/L_{298}$=0.0013, from NiO (Ref. 32).

tor, $S^2_{o,\text{eff}}$. We use the coordination number which is obtained in diffraction studies to calibrate the amplitude of the theoretical XAFS function, by fitting the calculated XAFS function to the experimental standard. Overall amplitude errors in $\exp[-2R_j/\lambda(k)]$ are included in $S^2_{o,\text{eff}}$, but distortions in the shape will remain. The values of $S^2_{o,\text{eff}}$ obtained are listed in Table II for the 27 isolated pair standards. Several points should be noted.

(1) Different k weighting could affect the value determined for $S^2_{o,\text{eff}}$, σ, and r, but this variation is quite small as shown in Table II; the rms variation of each parameter in our fits for the three k weightings is shown as a ± variation. However, the estimated errors (from χ-squared fits) for $S^2_{o,\text{eff}}$ are somewhat larger, about $\lesssim$ 5–6 % (see Sec. V F). In principle, the values of the parameters should not strongly depend on the k weight if the shape of the XAFS function has not been distorted and the signal-to-noise ratio is high. When the value of $S^2_{o,\text{eff}}$ and other parameters is not sensitive to the k weighting, the agree-

ment between the experimental and theoretical standards is generally much better.

Some values for $S^2_{o,\text{eff}}$ are available in the literature: 0.845 for Cu-Cu,[7] 1.00 for Rb-Br in RbBr,[19] 0.89 for Br-Rb in RbBr,[19] and 0.893 for Pt-Pt,[7] all of which are in good agreement with our results within the estimated uncertainty except for the Rb-Br pair in which our number (1.2) seems too large, perhaps due to the large Debye-Waller factor, 0.09 Å, or a difference in the "mean-free path" term.

(2) Excluding Rb-Br, $S^2_{o,\text{eff}}$ varies from 0.64 to 1.1, depending on the type of atom pair. $S^2_{o,\text{eff}}$ is about 0.84 for light metal pairs in elements such as Ni and Cu; $\sim$ 1.0 for median Z ($Z \simeq$ 40–51) metal pairs such as Zr-Zr, Nb-Nb, Ag-Ag, Cd-Cd, Cd-Te, In-Sb, Sn-Nb, and Sb-Nb; and 0.87 (at the L_{III} edge) for heavy metal pairs in elements such as Au and Pt. In Fig. 7 we plot the Z dependence of $S^2_{o,\text{eff}}$ which shows a wide range of values
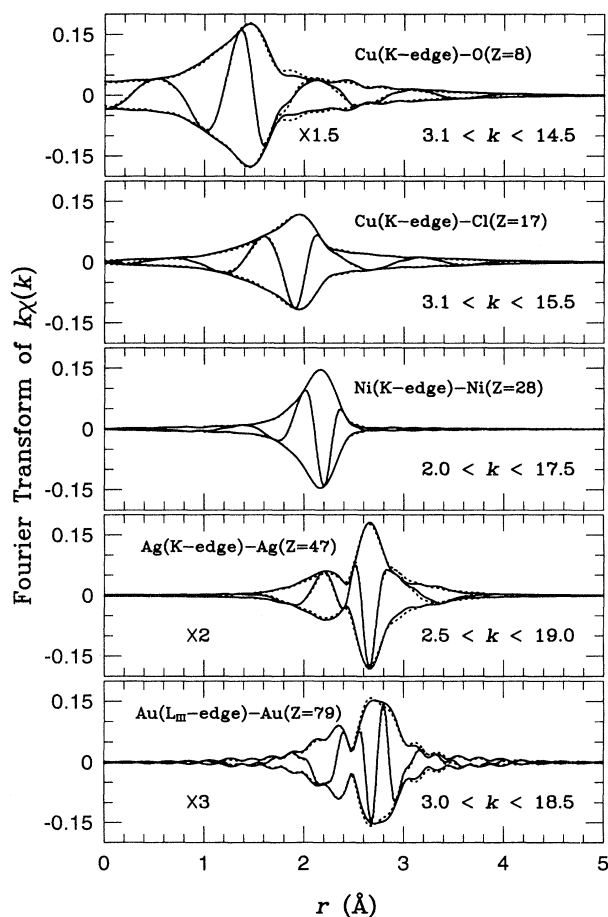

FIG. 4. Fourier transforms of $k\chi(k)$ for the Cu-O (in Cu_2O), Cu-Cl (in CuCl), Ni-Ni (in Ni), Ag-Ag (in Ag), and Au-Au (in Au) pairs. The solid lines are the experimental data and the dotted lines the fits to the data using the FEFF standards. Both the magnitude and the real part of the transform are plotted. The Fourier transform ranges are indicated and Gaussian rounded by 0.3 Å^{-1}.
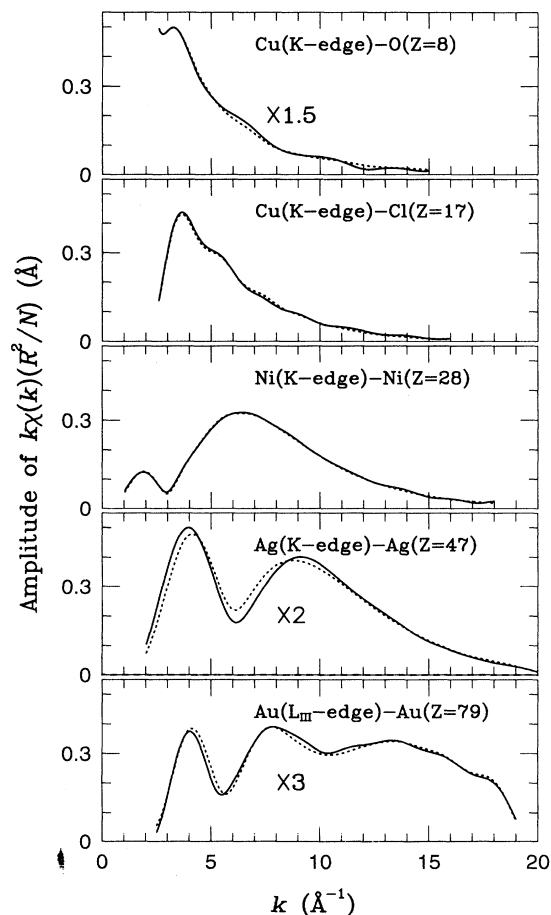

FIG. 5. Amplitude functions, $k\chi(k)(R^2/N)$ [which is the same as $A(k)$ in Eq. (3)] for Cu-O (in Cu_2O), Cu-Cl (in CuCl), Ni-Ni (in Ni), Ag-Ag (in Ag), and Au-Au (in Au) pairs. The solid lines are the experimental data and the dotted lines the fits to the data using the FEFF standards. The amplitudes are increased by the indicated factors for the Cu-O, Ag-Ag, and Au-Au pairs, to put all data on the same vertical scale.
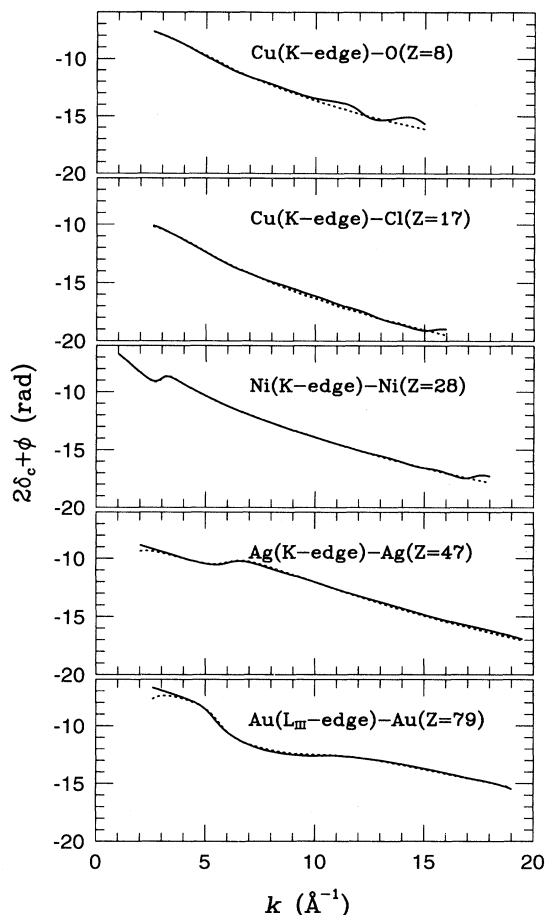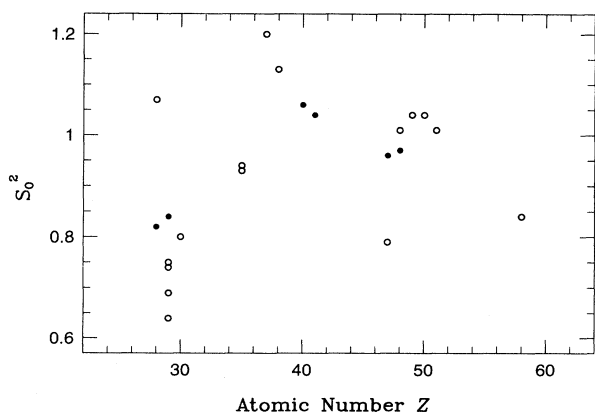
FIG. 6. Phase functions $[P(k) = 2\delta_c + \phi]$ for the Cu-O (in Cu_2O), Cu-Cl (in CuCl), Ni-Ni (in Ni), Ag-Ag (in Ag), and Au-Au (in Au) pairs. The solid lines are the experimental data and the dotted lines the fits to the data using the FEFF standards.

FIG. 7. Variation of $S_{o,\text{eff}}^2$ as a function of Z for the K edge experimental standards. Note that for some atoms there is a large difference in $S_{o,\text{eff}}^2$ for different crystal environments. The solid circles are for the pairs of metal atoms which are neighbors in the Periodic Table.

for Cu but a generally smooth variation with Z above $Z = 35$; i.e., the variation with Z is systematic [see point (4) below].

(3) There are six single-element samples — these samples happen to be composed of three pairs that are neighbors in the Periodic Table. Since these pairs are each metallic and have similar Z's, we expect that they will have similar $S_{o,\text{eff}}^2$'s, and they do: for Ni and Cu ($Z = 28$ and 29), $S_{o,\text{eff}}^2 = 0.82$ and 0.84; for Zr and Nb ($Z = 40$ and 41), $S_{o,\text{eff}}^2 = 1.06$ and 1.04; for Ag and Cd ($Z = 47$ and 48), $S_{o,\text{eff}}^2 = 0.96$ and 0.97. This is only a 2% variation between neighboring elements, consistent with our estimate that the errors in amplitude are 5–6% (see Sec. V D), but it is a 20% variation over this range of Z (28–48).

(4) It appears that $S_{o,\text{eff}}^2$ depends on the atomic number of the absorbing atom and usually can be treated as an overall amplitude correction factor for all the shells in a given simple compound. However at the 10–15 % level, Table II clearly shows that the $S_{o,\text{eff}}^2$ factor not only depends on the absorbing atom, but also varies with the local, chemical environment, as discussed in more detail in Sec. V C. In addition, note that S_o^2 should not be greater than unity. The authors of FEFF6 have suggested[10] that the mean-free path calculated by FEFF is often too small and can lead to values of $S_{o,\text{eff}}^2$ greater than unity. This together with errors in calculating $\exp[-2R_j/\lambda(k)]$ (which involves the imaginary part of the self-energy) may lead to values of $S_{o,\text{eff}}^2$ greater than unity. Figure 7 suggests that the errors in the total self-energy vary systematically with Z; there is a peak in $S_{o,\text{eff}}^2$ near Kr ($Z = 36$) where the $4p$ shell is filled, and another at Cd ($Z=48$) where the $5s$ shell is filled. Clearly more data is needed to determine this dependence.

Finally, in Table I we have compared our experimental values for σ with those calculated by FEFF5 for each shell (using the known Debye temperature) in Ni foil, NiO, and Au. Similar comparisons for some of the metal standards (first neighbor only) are reported in Table II. In six of nine comparisons, our experimental values for σ in the first shell are smaller than that calculated in FEFF5; in one case they are essentially the same (Cd), while in Zr and NiO, the experimental value of σ is larger. Most of the deviations are small, typically in the range 3–6 %, with the largest disagreements being for Pt and Au, 12–13 %. For the further neighbors the trend is reversed; the experimental values for σ are generally larger than the FEFF5 values and the deviation increases for the more distant shells.

B. Energy resolution

For double crystal monochromators, the x-ray energy is selected by Bragg's law, $2d(\text{Å}) \sin\theta = \frac{12.4}{E(\text{keV})}$, where d is the spacing of the crystal lattice planes, E is the photon energy, and θ is the angle between the incident ray and the reflecting plane. Thus the energy resolution is given by $\frac{\Delta E}{E} = \Delta\theta \cot\theta$. In XAFS measurements, the energy resolution is primarily determined by the angu-

lar spread of the x-ray beam $\Delta\theta$ and the Bragg angle θ (the Darwin natural width contributions are small). In practice, $\Delta\theta$ is approximately determined by the geometry of the experimental setup and can be estimated by $\Delta\theta = a/L$, where a is the vertical exit slit height of the monochromator and L is the distance between the x-ray source and the slit. A typical value of L for XAFS experiments at SSRL is about 20 m; the values of a used in most of our experiments range from 0.3–1.0 mm, which correspond to $\Delta\theta$ of 0.015–0.05 mrad. The calculated energy resolution, using Bragg's law and $\Delta\theta =0.05$ mrad, is shown in Fig. 8 as a function of energy for several Si crystals; we include this figure for comparison with the results below. In principle, there is also broadening from the source size. However, the electron beam size is approximately 0.1 mm in diameter; this means that source size broadening is generally a tiny contribution, less than 2 eV.

It has been recognized for a long time[28,29] that a loss of energy resolution tends to smear out the XAFS oscillations (reduce the amplitude) but the effect is often assumed to be unimportant because the experimental standards used to fit the data usually have approximately the same broadening. However if accurate amplitude and Debye-Waller factors are required, the loss of energy resolution as a result of using wide slits can be very important if the standards do not have the same broadening. As an illustrative example, we plot in Fig. 9, the amplitude of the Au-Au pair (r=2.88 Å) as a function of k for different values of ΔE. The amplitude of the XAFS function is nearly unchanged for ΔE=5 eV, slightly reduced for ΔE=10 eV, and significantly depressed for ΔE=15 eV. This effect is smaller for small r. Poor energy resolution depresses the amplitude of the XAFS function more in the low-k region than that in the high-k region and acts somewhat like a negative Debye-Waller effect. Based on Figs. 8 and 9, the energy resolution effect on our XAFS standards is expected to be negligible for $\Delta E \leq 5$ eV but could be important in some cases for data collected at the K edge of absorbing atoms heavier than Zr (Z=40, E_o=18 keV), and for more distant neighbors.

To check the effect of energy resolution, we broadened all the theoretical standards for elements with $Z \geq 40$ us-
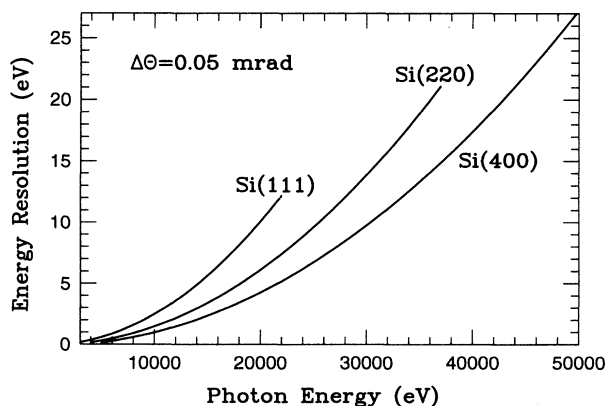

FIG. 8. Energy resolutions for various Si crystals, calculated using $\Delta E = E \cot\theta\Delta\theta$ with $\Delta\theta = 0.05$ mrad.
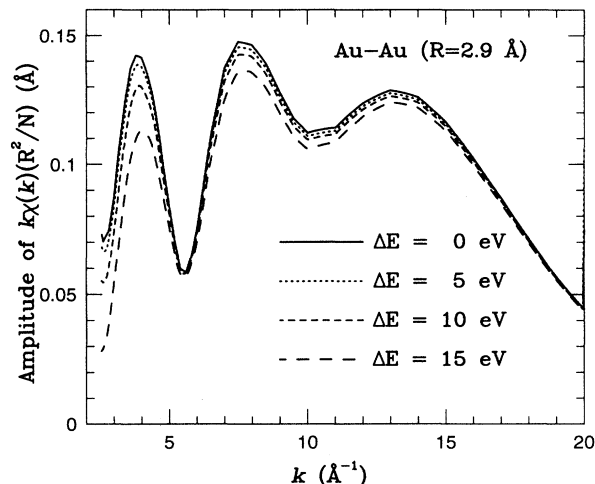

FIG. 9. Energy resolution effect on the amplitude of the Au-Au pair at $R = 2.9$ Å. Note the depression of the amplitude is greatest at low k.

ing the appropriate experimental $\Delta\theta$ (0.02~0.08 mrad, which corresponds to slit heights between 0.4~1.6 mm) by convoluting the FEFF standard with a square energy-resolution window, and then fitting these modified standards to the corresponding experimental ones. Broadening the theoretical standards had a negligible effect for the Ag-Ag, Ag-I, and Cd-Cd pairs and consequently, did not improve the quality of the fit; however, the broadened theoretical standards did improve the fits slightly for the Nb-Nb, Cd-Te, and Ce-O pairs. More importantly, the fits were significantly improved using the broadened theoretical standards for a few experimental standards extracted from old data collected using wide slits; specifically the Zr-Zr, In-Sb, Sn-Nb, and Sb-Nb pairs. An example is shown in Fig. 10 for the Sn-Nb pair, where a $\Delta\theta$ of 0.08 mrad (21~23 eV) was used. Note that the shape of the standard in r space is significantly improved; without this correction, the experimental and theoretical curves clearly have different shapes which limits the χ-squared fitting procedure. Using these broadened standards, the $S_{o,\mathrm{eff}}^2$ factor also increases (see Table III), while the dependence of $S_{o,\mathrm{eff}}^2$ on k weighting significantly decreases. These results clearly show that to obtain the correct shape, it is necessary to either use narrow slits or apply the broadening correction; for the higher energy edges, even with narrow slits, it is important that the standard (or the data) be corrected appropriately.

C. Dependence of $S_{o,\mathrm{eff}}^2$ on local environment

Table II and Fig. 7 show that the value of $S_{o,\mathrm{eff}}^2$ for a given absorption edge is also dependent on the local chemical environment. For example, $S_{o,\mathrm{eff}}^2$ is significantly smaller for Cu-O, Cu-Cl, and Cu-I than it is for Cu-Cu; similar magnitude changes are observed for Ag-I and Ag-Ag pairs, while for the Ni edge, Ni-O has a much larger value for $S_{o,\mathrm{eff}}^2$ than Ni-Ni in Ni foil. Thus if reasonably accurate values for the number of neighbors are required,
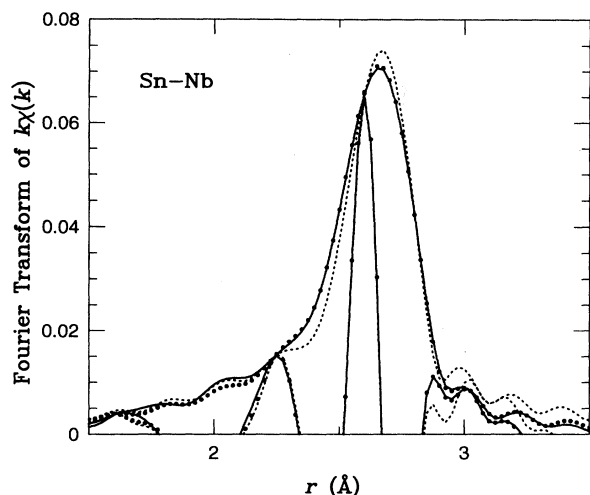
FIG. 10. Fourier transforms of $k\chi(k)$ for the Sn-Nb pair in Nb$_3$Sn. The transform windows are from 3.5 to 18.5 Å^{-1}, Gaussian rounded by 0.3 Å^{-1}. Solid lines, the experimental data; dotted lines, fits to the data using the FEFF standards; bold dots, fits to the data using the resolution-broadened FEFF standards with $\Delta\theta = 0.08$ mrad. See Sec. V B.

it is necessary to know how $S^2_{o,\text{eff}}$ varies with the local environment for a given atom pair.

We first considered how the theoretical standards change with the local environment, and calculated (using FEFF5) the XAFS spectra for Cu-O pairs in several different environments: (i) $r=1.841$ Å (in Cu$_2$O), (ii) $r=1.857$ Å [Cu(1)-O(4) in YBa$_2$Cu$_3$O$_7$], (iii) $r=1.951$ Å (in CuO), and (iv) $r=1.933$ Å (in Tl$_2$Ba$_2$CuO$_6$). A Debye-Waller factor of 0.04 Å has been included in each spectra and the mean-free path term calculated by FEFF5 is also included. The amplitude functions of $k\chi(k)$ (normalized to one atom) are plotted in Fig. 11. Clearly the amplitude of the Cu-O pair standard is lower in cuprous and cupric oxides than it is in the high-T_c materials for k less than 6 Å^{-1}. To obtain a quantitative comparison, we Fourier transformed these theoretical XAFS standards from 3.0 to 14.5 Å^{-1} using a Gaussian rounding of the transform window of 0.3 Å^{-1}. Next we fit in r space (from 0.8 to 3.2 Å), the XAFS function for the oxide to

TABLE III. The change in $S^2_{o,\text{eff}}$ with and without the correction for energy resolution broadening; the FT ranges are given in Fig. 4. Note that $S^2_{o,\text{eff}}$ increases when the correction is applied and that for high energy edges such as the Ce K edge, a very small angular spread of the beam (slit height = 0.4 mm) gives an observable correction.

Atom pair	$\Delta\theta$ (mrad)	$S^2_{o,\text{eff}}$ (uncorrected)	$S^2_{o,\text{eff}}$ (corrected)
Zr-Zr	0.08	1.02	1.06
Nb-Nb	0.06	1.03	1.04
Cd-Te	0.05	0.94	1.01
In-Sb	0.05	0.94	1.04
Sn-Nb	0.08	0.82	1.04
Sb-Nb	0.04	0.93	1.01
Ce-O	0.02	0.82	0.84
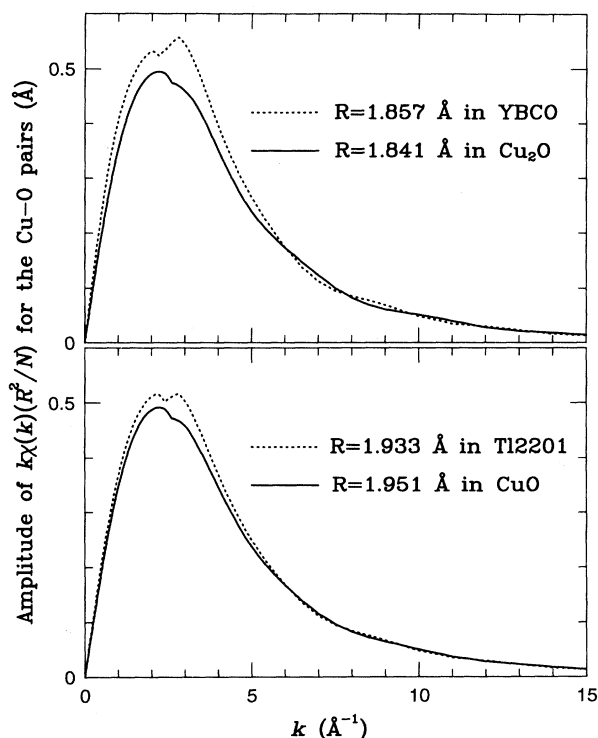
FIG. 11. Amplitude functions of $k\chi(k)(R^2/N)$ for the Cu-O pairs calculated in YBa$_2$Cu$_3$O$_7$ (YBCO), Cu$_2$O, Tl$_2$Ba$_2$CuO$_6$ (Tl2201), and CuO, using the FEFF5 code and 7-Å-radius clusters. A Debye-Waller factor of 0.04 Å is included. See Sec. V C.

the function generated for the high-T_c material of nearly the same Cu-O bond length ($\Delta r < 0.02$ Å) — i.e., case (i) to case (ii) and case (iii) to case (iv) above. The resulting fits show that the amplitude of the Cu-O standards for Cu$_2$O and CuO are about 10–16 % lower than for the corresponding superconductor standard. The difference in amplitude decreases with higher k weighting, 7–10 % for k^2 weighting, 4–6 % for k^3 weighting, as expected from Fig. 11. These simulations indicate that there is clearly a local environment effect for the same pair of atoms, particularly at low k.

Next we fit the calculated Cu-O standard, $k\chi(k)$, to the experimental one for Tl-2201,[21] which has a single, well defined Cu site. A comparison of the XAFS and diffraction results yields $S^2_{o,\text{eff}} = 0.76$. Similarly, we fit [again for $k\chi(k)$] the calculated Cu-O standard to the experimental one for the CuO environment (with $r=1.95$ Å). For this fit we obtain $S^2_{o,\text{eff}} = 0.64$, significantly smaller than that in Tl-2201. Note that although the amplitude difference in the theoretical standards at low k has been included in these fits, it is not enough to keep $S^2_{o,\text{eff}}$ constant. The results for this one atom-pair case suggests that the theoretical calculations do not completely correct for local environmental variations. However a number of such comparisons need to be made to clarify how large and how important this amplitude effect is overall.

For atom pairs with the same central atom but a different backscattering atom (in different compounds), there

is sometimes a large change in $S_{o,\text{eff}}^2$; compare the $S_{o,\text{eff}}^2$ results for NiO and Ni foil at the the Ni K edge and AgI and Ag foil at the Ag K edge in Table II. Yet in other examples the change is small — for instance, in Br-Cu (CuBr) and Br-Rb (RbBr). Again careful comparisons for a large number of pairs are needed to clarify the problem. However, it appears that these changes are determined by the local environment (i.e., the compound) and not so much the change in the backscattering atom. Consider the results for NiO and Ni foil in Table I, where the amplitudes for the further neighbors are also given. In these fits there is only one value of $S_{o,\text{eff}}^2$ used for the sample: 0.82 for all shells in Ni foil and 1.04 for all shells in NiO. One value works quite well for all shells. In each case the second neighbor is Ni. Clearly using $S_{o,\text{eff}}^2$ = 0.82 (from Ni foil) for the Ni-Ni second neighbor pair in NiO would give too large a value for the number of second neighbors by $\sim 23\%$. On the other hand, $S_{o,\text{eff}}^2$ = 1.04 (the value of $S_{o,\text{eff}}^2$ for Ni-O of the first shell) is only 5% high.

D. Amplitude and phase functions

The amplitude and phase functions for five typical pairs are plotted as a function of k in Figs. 5 and 6, with the backscattering atoms chosen from five different rows (second to sixth rows) in the Periodic Table. Overall, the agreement in phase and amplitude is very good. Some particular features include the following.

(1) For pairs with the backscattering atoms in the second and third rows, the agreement is excellent in both the phase and amplitude for k less than 11 Å^{-1}. The experimental XAFS function is not as well determined for $k \gtrsim 11$ Å^{-1} as in the range $4 \sim 10$ Å^{-1}, due to the low magnitude of the backscattering function $F(k, R)$. Consequently, small errors in the high-k region do not degrade the quality of the r space data analysis much for the FT of $k\chi(k)$, because the high-k region does not contribute much to the r space peak.

(2) The agreement between the experimental data and theoretical standards is excellent for pairs with the backscattering atoms in the fourth row (Ni, Cu, etc.).

(3) Small but systematic discrepancies exist for some pairs with the backscattering atoms in the fifth row. In r space, the standards for these pairs appear as a "double peak" because of a sharp dip in $F(k, R)$ (a Ramsauer-Townsend effect from the backscattering atom). In our studies, the low-r peak of each "double peak" standard is systematically higher in the experimental standards for pairs such as Nb-Nb, Ag-Ag, Cd-Cd, In-Sb, Zn-Te, Hg-Te, and Cu-I . In k space, those pairs have two peaks in $F(k, R)$; the lower-k peak is usually higher in the experimental standards than that in the theoretical ones. An example (Ag-Ag) is shown in Fig. 4.

(4) There are small but distinct differences between the experimental XAFS standards and theoretical ones for pairs with heavier backscattering atoms such as Pt and Au. An example is shown in Figs. 4–6 for the Au-Au pair. In r space, there are significant discrepancies near the top of the main peak; the discrepancies can be greatly enhanced using a low-k-region Fourier transform.

In k space, the shape of the phase function agrees very well but the amplitude function does not in the range of $4 \sim 10$ Å^{-1}. The discrepancy in the r space amplitude can be minimized if a constant phase shift is added to the phase function in the theoretical standards as a fitting parameter. When the phase shift was allowed to vary but kept equal for all the shells in the fit to the Au foil data, the resultant phase shift was -0.25 rad and C^2 decreased; see Table I for a list of the parameters. When an isolated Au-Au pair is fit, the phase shift is about -0.6 rad. The quality of the fit when the phase shift was included improved greatly as shown in Fig. 12; the discrepancy near the top of the main peak has almost disappeared. The value of ΔR is comparable to that given in Table II.

E. Transferability of experimental standards

Since the theoretical (FEFF) XAFS standards for some heavier backscattering atoms ($Z \lesssim 41$) are not as good as for light backscattering atoms we have found that it is better to use experimental standards for these pairs. However, a corresponding experimental standard is not always available. One way to overcome this problem is to shift one experimental standard to another by using theoretical results. We and others have used this approach for a number of years but generally the quality of the generated standard is not reported in the detail that we present here.

As an example, we modify an experimental Pt-Pt pair standard to generate a Au-Au pair standard to show the high quality of this procedure. First, the theoretical stan-
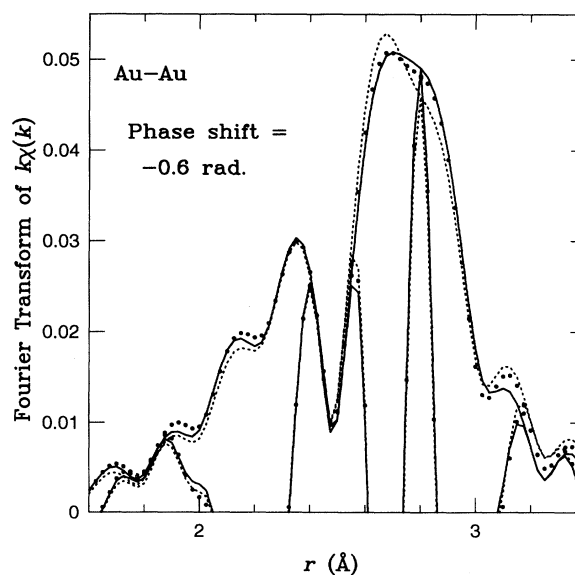
FIG. 12. Fourier transform of $k\chi(k)$ for the Au-Au pair in Au. The transform range is the same as that in Fig.4. Solid lines, the experimental data; dotted lines, fits to the data using the FEFF standards; bold dots, fits to the data using the FEFF standards with the phase function shifted by -0.6 rad. See Sec. V D.

dards for Pt-Pt and Au-Au are generated using the FEFF code for an atomic cluster which includes all atoms within 7 Å from the center atom. Then the amplitude and the phase functions of the Pt-Pt pair standard are modified to generate the new ones for Au-Au, using

$$A_{\text{Au-Au}}^{\text{new}} = A_{\text{Pt-Pt}}^{\text{exp}} A_{\text{Au-Au}}^{\text{FEFF}} / A_{\text{Pt-Pt}}^{\text{FEFF}} \tag{5}$$

and

$$P_{\text{Au-Au}}^{\text{new}} = P_{\text{Pt-Pt}}^{\text{exp}} + P_{\text{Au-Au}}^{\text{FEFF}} - P_{\text{Pt-Pt}}^{\text{FEFF}}. \tag{6}$$

This new Au-Au standard fits the experimental Au data much better than the theoretical standard does, as shown in Fig. 13(a). The agreement is improved significantly not only for the highest peak, but also over the entire region of r space. The extracted fitting parameters now agree extremely well with the known values for Au; the error is about 3% in amplitude and 0.001 Å in distance, much better than the fit obtained using the theoretical standard. Similarly, the fit to the Ag-Ag data can be greatly improved by using a standard generated from the Cd-Cd pair standard.

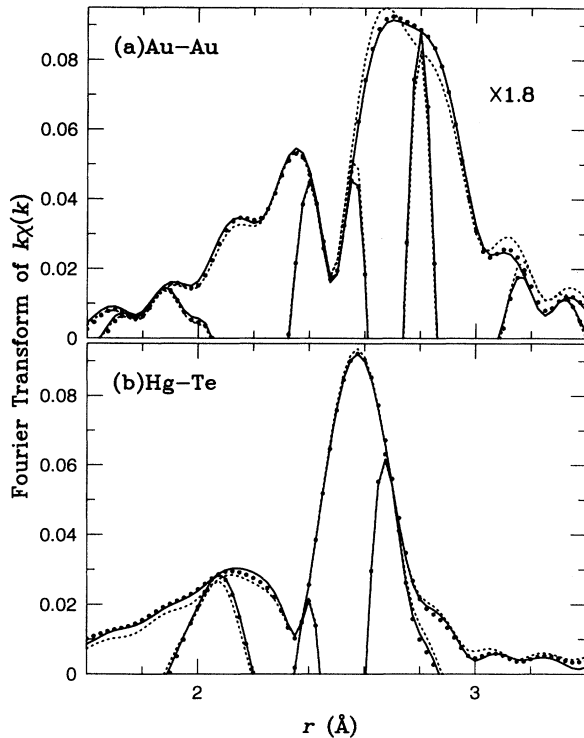One can sometimes even shift a pair standard from the

FIG. 13. Fourier transform of $k\chi(k)$ for (a) the Au-Au pair in Au and (b) the Hg-Te pair in HgTe. Solid lines, the experimental data; dotted lines, the fits to the experimental data using the FEFF standards; bold dots, the fits to the experimental data using the modified experimental (a) Pt-Pt and (b) In-Sb pair standards, respectively. The transform range is from 3.0 to 18.5 Å^{-1} for Au-Au and 2.8 to 19 Å^{-1} for Hg-Te, Gaussian rounded by 0.3 Å^{-1}. The magnitude of the transform for Au-Au is increased by a factor of 1.8 to be on the same scale.

K edge to the L_{III} edge to yield a better fit. For example, the K edge In-Sb pair standard can be shifted to the L_{III} edge Hg-Te pair standard. The agreement improved as shown in Fig. 13(b). The error in the extracted distance is again only about 0.001 Å. However, due to the large difference in $S_{o,\text{eff}}^2$ between the Hg-Te and In-Sb pairs, the error in amplitude is still large, $\sim 20\%$. Similarly, the error in the fit to the Cu-I data can be minimized by using a standard generated from the Hg-Te experimental standard.

In our experience, the Z of the central absorbing atom can be shifted a long way in the Periodic Table, and from one edge to another, in generating a new standard. This is probably due to the fact that the amplitude function does not strongly depend on the absorbing atom and the central atom phase shift function varies smoothly with k. However, the amplitude functions for heavy backscattering atoms are strongly Z dependent and have sharp peaks and dips in k space. Consequently, the shift (ΔZ) of the backscattering atom in such standards, should generally be limited to about $\Delta Z \simeq 4$ for high-Z backscatterers.

F. Correlations and uncertainties

It is generally recognized that there are two sets of variables that can be highly correlated: $\{N, \sigma\}$ and $\{\Delta E_o, R\}$. For example, starting from an optimal fit an increase in σ will cause an attenuation over the entire XAFS spectrum; in order to best fit the data, N must be increased accordingly. Similarly, ΔE_o and R are correlated to some extent even though they have different k dependences; δE_o mainly shifts the phase of the XAFS function at low k while R still has a strong influence on the high-k region. These correlations can lead to additional uncertainties for the extracted XAFS parameters (often the dominant uncertainty), especially in a complicated system where different shells may totally overlap in r space.

The absolute error in pair distances, R, obtained from XAFS for the experimental standards, is estimated by comparing XAFS values with the corresponding values from diffraction studies. The error for the nearest-neighbor distance is typically about 0.005 Å. Since the k range of our data is quite large, typically $3 \sim 16$ Å^{-1} or longer, the effects of the correlation between ΔE_o and R are not strong. This can be seen from the weak k weighting dependence of the ΔR and ΔE_o values listed in Table II. We address the correlation between ΔE_o and R after discussing the larger effects from the correlations between N and σ.

In order to gain a better understanding for the uncertainties and the correlations in N and σ, and also the errors in the theoretical standards, we varied the fitting parameters R, ΔE_o, and σ for the Au-Au experimental standard, keeping the amplitude, N, fixed at several different values around the optimum point, N_o. We used two different standards: the theoretical FEFF5 standard, and the standard generated from Pt-Pt as outlined above. A plot of C^2 as a function of the normalized amplitude, N/N_o, is shown in Fig. 14. The minimum value, C_o^2, is an order of magnitude smaller using the experimental
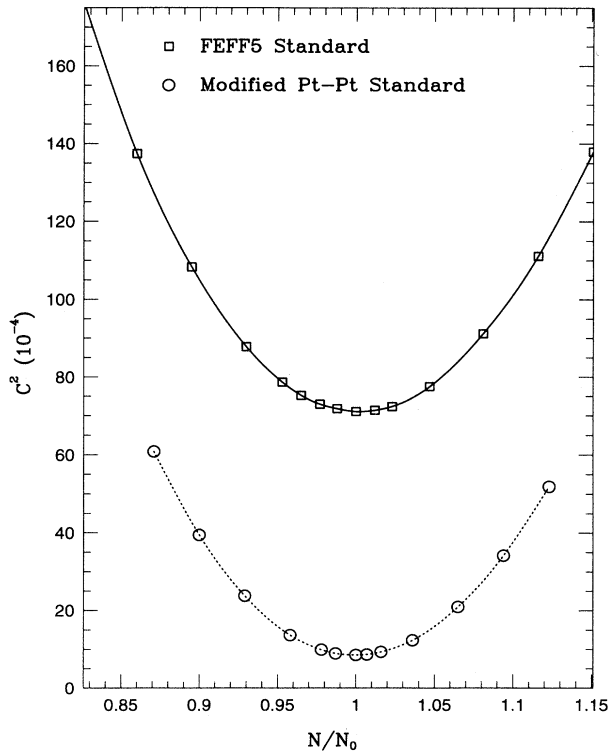
FIG. 14. A plot of C^2 for various values of N/N_o for the nearest-neighbor peak in Au foil. Two standard functions were used: an FEFF5 standard and a modification of the Pt-Pt experimental standard using the FEFF5 theoretical results ($\Delta Z = 1$). The latter gives a much better fit to the data.

standard, and should give much smaller errors for the parameter N. (Note that here one clearly cannot use the errors from the data in estimating the errors on the fit parameters when using the theoretical standards.) Interestingly, the curvature is nearly the same for both curves. This appears to be a universal result for the amplitude variable for good S/N: the shape of the curve in Fig. 14 is determined by the general shape of a particular standard in r space (and on the chosen r and k ranges), and not by the S/N. Thus for comparison purposes we will plot $C^2 - C_o^2$ vs N/N_o. We chose five pairs as examples, with the backscattering atoms from different rows in the Periodic Table (from the second to the sixth row) to obtain some global perspective. Note that if we normalized C^2 by C_o^2 instead of subtracting it, the curvature would be high when C_o^2 is small and visa versa.

1. Uncertainties in N

In Fig. 15(a), $C^2 - C_o^2$ is plotted as a function of N/N_o for the fits to five experimental atom-pair standards, where C_o^2 and N_o are the optimum values when all four fitting parameters (N, σ, R, ΔE_o) are free to vary. [C_o^2 is usually between $1-20 \times 10^{-4}$ for Eq. (2).] All fits were carried out using FEFF5 standards, and in this set of results, N was fixed and the other three parameters varied. The FT ranges were the same as those in Fig. 4.
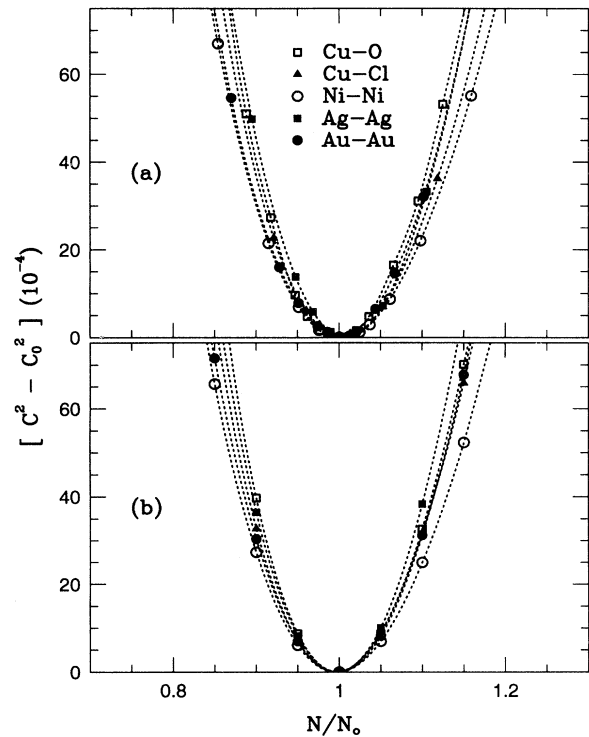

FIG. 15. The relative quality of fit parameter, $C^2 - C_o^2$, as a function of variations in the normalized amplitude, N/N_o, obtained from (a) the experimental data and (b) simulations. See Sec. V F.

For the range of N used, the changes in R and ΔE_o were insignificant; thus each of these fits is essentially a one parameter fit for σ, with N fixed.

To compare with theoretical standards we first generated a "noiseless" data file for each pair by broadening the theoretical standard with a Debye-Waller factor σ identical to the real data as listed in Table II. These files were then fit the same way as the five experimental data files described above. In this case because the data are noise-free C_o^2 is very close to zero. The results from these fits are plotted in Fig. 15(b).

Several general features emerge from Fig. 15. First the width of the curves in Figs. 15(a) and 15(b) do not change much from one atom pair to another; the curvature varies less than a factor of 2, and has nearly the same range of values for the different atom pairs in the "noiseless" data [Fig. 15(b)] as in the real data. Second, the curves are slightly asymmetric (especially Au); the same asymmetry is observed for both the "noiseless" data and the real data. Third there is a small systematic change of the curvature in Fig. 15(b) — the curvature is smallest for Ni (although it has the narrowest peak in r space), and is largest for Ag and O. This trend is also observed in the real data. Some of these results are as expected. If the fit [see Eq. (2)] uses the same weighting and the same fitting function, then the curvature for $C^2 - C_o^2$ vs N/N_o is determined by the shape of the model function as long as the S/N is reasonable. It is not so obvious, however, that the curvature should vary so little with different

atom pairs, since it should depend on the Debye-Waller factor used, the k range of the FT, the fit range in r space, and the shape of the function $F(k, R)$.

The error in the amplitude parameter is usually determined from a fractional increase of C^2 above C_o^2. This fraction depends on the estimated errors, the number of parameters, the fit ranges, etc.; typical increases may be 50 to 100%. The results in Fig. 15 indicate that comparable accuracy (within a factor of 2) should be possible for most atom pairs if good S/N is achieved (i.e., a low value of C_o^2 is obtained). Thus we emphasize the need to use the best available standards to minimize their contributions to the error. The estimated uncertainty in N is about 5–6 % for most pairs in our study, and $\sim$ 3–4 % for pairs such as Ni-Ni, Cu-Cu, Cu-Br, and Br-Cu.

2. Uncertainties in σ

In a similar manner, we calculated the variation of $C^2 - C_o^2$ as a function of $\delta\sigma = \sigma - \sigma_o$, for the same experimental and "noiseless" data files used in Fig. 15. These results are plotted in Fig. 16. Again, the shape of the curve is almost the same for the real and "noiseless" data. More importantly, there is a wide variation of the resulting curvature, which varies systematically with the atomic number of the backscattering atom. The curvature is very large for Au-Au and small for Cu-O; consequently, the errors in σ will be much larger for Cu-O

than for Au-Au. This variation appears to depend on the contributions to the FT at high k, and thus is determined both by the FT range and the shape of the function $F(k, R)$. σ has the largest effect at high k; consequently for a large backscattering amplitude and a long FT range a small change in σ will cause a significant change in C^2. Conversely, for Cu-O, which has very little amplitude above 12 Å^{-1}, variations in σ produce a much smaller change in C^2.

A final comment for errors in σ concerns the fit range R. In many spectroscopies, much of the information about the width is contained in the wings of the peak. The same is true for XAFS, even though the relatively short FT range usually available broadens the overall envelope of the r space peak. We fit to the real and imaginary parts of the FT and are therefore very sensitive to the zero crossings of these functions. When σ is increased the separation between zero crossings in r space increases. Thus if the S/N is good enough to include the wings of the r space peak the fit is much more sensitive to σ, and the effect of the correlation between σ and N is decreased.

3. Correlations between N and σ

From the same fits used to generate Figs. 15 and 16, we also determined N/N_o as a function of $\sigma - \sigma_o$. These results are plotted in Fig. 17. The curves for the real data [Fig. 17(a)] and "noiseless" data [Fig. 17(b)] are
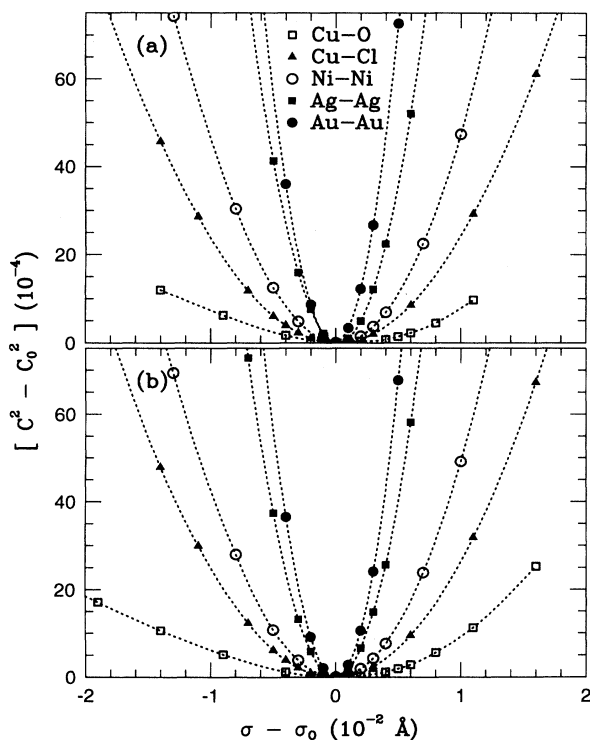

FIG. 16. The relative quality of fit parameter, $C^2 - C_o^2$, as a function of variations in the Debye-Waller factor, $\sigma - \sigma_o$, obtained from (a) the experimental data and (b) simulations. See Sec. V F.
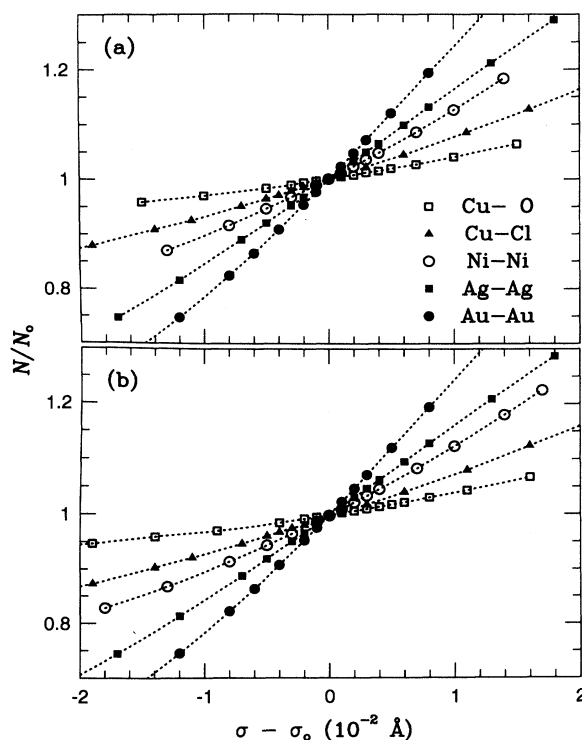

FIG. 17. Correlations between the amplitudes and the Debye-Waller factors in XAFS data analysis, obtained from (a) the experimental data and (b) simulations. See Sec. V F.

essentially the same. All are close to straight lines, which indicate a clear correlation between N and σ in the data analyses. However, this plot is a little misleading as the values of C^2 and C_o^2 are not given, and in some cases C^2 is very large. Contours of constant C^2 should be added to provide a scale for estimating the importance of the correlations; these contours are different for each atom pair.

The slope of the lines in Fig. 17 change systematically with the backscattering atom; 3.5 Å^{-1} for O (Z=8), 6.3 Å^{-1} for Cl (Z=17), 10 Å^{-1} for Ni (Z=28), 15 Å^{-1} for Ag (Z=47), and 23 Å^{-1} for Au. Although these results should depend on the k space FT range, we found empirically, for the ranges chosen, that the functional dependence of the slope on Z can be reasonably parameterized by a straight line,

$$\Delta\left(\frac{N}{N_o}\right)\Big/\Delta\sigma = 1.6 + 0.27Z. \qquad (7)$$

Thus, for a given $\Delta(\frac{N}{N_o})$, the corresponding uncertainty in σ can be estimated using $\Delta(\frac{N}{N_o})/(1.6 + 0.27Z)$ (in Å). For example, using this equation, the calculated $\Delta\sigma$ is 0.0023 Å for the Au-Au pair (Z=79), at $\Delta(\frac{N}{N_o})$=5%. From Fig. 15(a), the corresponding value of $C^2 - C_o^2 = 2\times 10^{-4}$; using this value in Fig. 16(a) gives $\Delta\sigma$ =0.002 Å consistent with the calculated result. Knowing the slope one can also define variables that are less correlated, but that is beyond the scope of this paper.

4. Correlations between R and ΔE_o

Following a procedure similar to that used above, we investigated the correlations between R and ΔE_o. In each fit, δR was set at a particular value ($\delta R = R - R_o$ where R_o is the best-fit value) and ΔE_o, N, and σ were allowed to vary. For small values of δR, only ΔE_o varies; N and σ are essentially constant. When δR is greater than approximately $\pm$ 0.03 Å, N and σ also begin to change. For all pairs studied the correlation between δR and $\delta(\Delta E_o)$ (the change in ΔE_o from its best-fit value) is negative as expected [see Fig. 18(a)]. However, the dependence is linear only over a small range of δR, roughly the range for which N and σ do not change significantly. For determinations of R, only this small range is important since C^2 changes very rapidly with δR as shown in Fig. 18(b). Using as a rough criteria that the error in R is determined by the value that doubles C^2, then the errors for all the standards shown in Fig. 18(b) are less than $\pm$0.02 Å and in many cases less than $\pm$ 0.01 Å. [At sufficiently large values of δR (with very large values of C^2) the values of $|\delta(\Delta E_o)|$ become smaller again and the function is not single valued.] In this sense we find that the effect of the correlation between R and ΔE_o is not important since the resulting error in R is small. On the other hand, it is very difficult to obtain accurate values of ΔE_o.

VI. SUMMARY

We have carried out a careful comparison between experimental and theoretical standards for 27 experimental standards that we have generated from reference compounds. Overall the quality of the fits is high indicating that the theoretical standards calculated from the FEFF5 program are good standards. In particular, the agreement is very good for atom pairs with $Z \lesssim 40$. In some cases—Ni and Cu—the fits are excellent while for other atom pairs (usually for the heavier backscattering atoms) there are small but clear systematic deviations between the theoretical and experimental r-space curves. We emphasize that it is the *shape* that differs between the theoretical and experimental standards, both in r and k space. In all cases considered, the k depen-
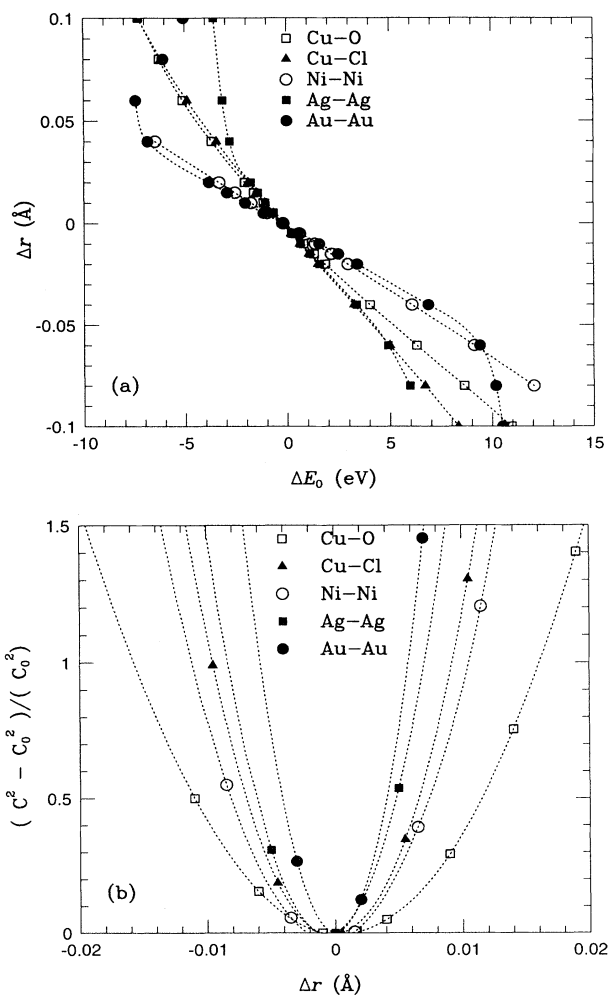

FIG. 18. (a) Correlations between r and E_0 are displayed for several atom-pairs. The correlation is only linear over a small range in ΔR. See Sec. V F. (b) Normalized C^2 vs ΔR for several pairs. Experimental uncertainties in the fit parameters can be conservatively estimated by taking the change in the parameter required to double C^2, i.e., the ΔR that corresponds to $(C^2 - C_0^2)/C_0^2 = 1$ on this plot. For the pairs plotted, the uncertainty in ΔR varies between 0.005 and 0.015 Å.

dence of the calculated phase agreed well with the phase extracted from the experimental data. Consequently, the main deviations occur for the backscattering amplitude, $F(k, R)$; significant differences generally occur when a sizable Ramsauer-Townsend effect is present in the backscattering atom, and possibly in the absorbing atom. In a few cases, a constant overall phase shift improved the fit. This difference in overall shape of the standard is one of the main areas that needs additional theoretical attention.

Often an experimental standard does not exist for a particular atom pair; then if the calculated FEFF5 standard does not fit well, an "experimental" standard can be generated by modifying another experimental standard, using the theoretical results. Generally this requires that the change in atomic number Z be small. As an example, we showed that the χ-squared fit to the Au-Au first neighbor peak was improved by nearly an order of magnitude when using a Au-Au standard generated from a Pt-Pt experimental standard, relative to the fits using the FEFF5 standard alone.

We have included extensive details about the data reduction and the extraction of each isolated pair standard from the reference compound XAFS data. In particular we have addressed the removal of the further neighbors and the distortions that occur from structure in the background above the edge (from multielectron excitations and atomic XAFS) and from energy resolution effects. All distortions of the isolated-atom standard result in a degradation of any χ-squared fit and must be minimized.

A comparison of the XAFS amplitude with the known number of neighbors provides an experimental number for the amplitude reduction factor. Since the FEFF5 standards also include an energy dependent mean-free path term and central-atom loss factor, the quantity we obtain is an effective correction factor $S^2_{o,\mathrm{eff}}$ which includes errors in the estimation of these quantities, as well as the expected reduction of the XAFS oscillations as a result of multielectron effects. For a given material, $S^2_{o,\mathrm{eff}}$ is about the same for all neighbors. However, it sometimes changes for different local environments, i.e., different compounds. Furthermore, our limited data set suggests that $S^2_{o,\mathrm{eff}}$ changes most rapidly with Z when a shell (i.e., $4p$ for Kr) is filled, and slowly otherwise. We speculate that this rapid variation is mostly due to problems in estimating the core-hole lifetime, but many-body effects may turn out to dominate. This is another area that requires further theoretical study.

Lastly, we have discussed the errors in σ and N and shown how the effects of correlations between these variables can be reduced. With high signal-to-noise data it is important to include the wings of the r space peak in the fit to improve the sensitivity to σ. We also note that in χ-squared fits the largest contributions to the parameter error often arise either from systematic errors in the standard used or from structure in the absorption background that has not been removed. Consequently, estimating the parameter error from the errors in the raw data may be incorrect.

[1] E. A. Stern and S. M. Heald, in *Handbook on Synchrotron Radiation*, edited by E. E. Koch (North-Holland, New York, 1983), Vol. 1, p. 955.

[2] T. M. Hayes and J. B. Boyce, in *Solid State Physics*, edited by H. Ehrenreich, F. Seitz, and D. Turnbull (Academic, New York, 1982), Vol. 37, p. 173.

[3] P. A. Lee and G. Beni, Phys. Rev. B **15**, 2862 (1977).

[4] B. Teo and P. A. Lee, J. Chem. Soc. **101**, 2815 (1979).

[5] A. G. McKale, B. W. Veal, A. P. Paulikas, S.-k. Chan, and G. S. Knapp, J. Am. Chem. Soc. **110**, 3763 (1988).

[6] S. J. Gurman, J. Phys. C **21**, 3699 (1989).

[7] J. Mustre de Leon, J. J. Rehr, and S. I. Zabinsky, Phys. Rev. B **44**, 4146 (1991).

[8] J. J. Rehr, J. Mustre de Leon, S. I. Zabinsky, and R. C. Albers, J. Am. Chem. Soc. **113**, 5135 (1991).

[9] J. J. Rehr, S. I. Zabinsky, and R. C. Albers, Phys. Rev. Lett. **69**, 3397 (1992).

[10] S. I. Zabinsky, J. J. Rehr, A. Ankudinov, R. C. Albers, and M. J. Eller, Phys. Rev. B **52**, 2995 (1995).

[11] F. Bridges and G. G. Li, Bull. Am. Phys. Soc. **39**, 664 (1994).

[12] E. A. Stern and K. Kim, Phys. Rev. B **23**, 3781 (1981).

[13] Kun-quan Lu and E. A. Stern, Nucl. Instrum. Methods **212**, 475 (1983).

[14] G. G. Li, F. Bridges, and X. Wang, Nucl. Instrum. Methods A **340**, 420 (1994).

[15] R. F. Pettifer, C. Brouder, M. Benfatto, C. R. Natoli, C. Hermes, and M. F. Ruiz López, Phys. Rev. B **42**, 37 (1990).

[16] G. G. Li, F. Bridges, and G. Brown, Phys. Rev. Lett. **68**, 1609 (1992).

[17] A. Filipponi, A. Di Cicco, T. A. Tyson, and C. R. Natoli, *GNXAS Package Documentation* (University Press, Camerino, 1992); A. Filipponi, A. Di Cicco, T. A. Tyson, and C. R. Natoli, Solid State Commun. **78**, 265 (1991).

[18] M. Newville, P. Livins, Y. Yacoby, J. J. Rehr, and E. A. Stern, Phys. Rev. B **47**, 14 126 (1993).

[19] A. I. Frenkel, E. A. Stern, M. Qian, and M. Newville, Phys. Rev. B **48**, 12 449 (1993).

[20] F. Bridges, C. Booth, and G. G. Li, Physica B **208&209**, 121 (1995).

[21] G. G. Li, F. Bridges, J. B. Boyce, T. Claeson, C. Ström, S.-G. Eriksson, and S. D. Conradson, Phys. Rev. B **51**, 8564 (1995).

[22] C. H. Booth, F. Bridges, J. B. Boyce, T. Claeson, Z. X.

Zhao, and P. Cervantes, Phys. Rev. B **49**, 3432 (1994).

[23] J. J. Rehr, C. H. Booth, F. Bridges, and S. I. Zabinsky, Phys. Rev. B **49**, 12 347 (1994).

[24] A. Filipponi, L. Ottaviano, and T. A. Tyson, Phys. Rev. A **48**, 2098 (1993); A. Di Cicco and A. Filipponi, Phys. Rev. B **49**, 12 564 (1994).

[25] B. K. Teo, *EXAFS: Basic Principles and Data Analysis* (Springer-Verlag, New York, 1986), p. 146.

[26] J. J. Rehr, E. A. Stern, R. L. Martin, and E. R. Davidson, Phys. Rev. B **17**, 560 (1978).

[27] T. A. Carlson, *Photoelectron and Auger Spectroscopy* (Plenum Press, New York, 1975), p. 79.

[28] P. A. Lee, P. H. Citrin, P. Eisenberger, and B. Kincaid, Rev. Mod. Phys. **53**, 769 (1981).

[29] B. Lengler and P. Eisenberger, Phys. Rev. B **21**, 4507 (1980).

[30] G. T. Furukawa, T. B. Douglas, and N. Pearlman, in *American Institute of Physics Handbook*, edited by D. E. Gray (McGraw-Hill, New York, 1972), pp. 4–115.

[31] *Landolt-Börnstein: Numerical Data and Functional Relationships in Science and Technology*, edited by K. H. Hell-wege and O. Madelung Group III, Vol. 17, Pt. g (Springer-Verlag, Berlin, 1984).

[32] R. W. G. Wyckoff, *Crystal Structures*, Vol. 1 (Interscience Publishers LTD., New York, 1960).

[33] R. K. Kirby, T. A. Hahn, and B. D. Rothrock, in *American Institute of Physics Handbook*, edited by D. E. Gray (McGraw-Hill, New York, 1972), pp. 4–119.

[34] L. Tröger, T. Yokoyama, D. Arvanitis, T. Lederer, M. Tischer, and K. Baberschke, Phys. Rev. B **49**, 888 (1994).

[35] T. Suzuki, J. Phys. Soc. Jpn. **15**, 2018 (1960).

[36] *Landolt-Börnstein: Numerical Data and Functional Relationships in Science and Technology*, Vol. 17, Pt. b (Springer-Verlag, Berlin, 1982).

[37] G. K. White and J. G. Collins, Proc. R. Soc. London Ser. A **333**, 327 (1973).

[38] *Landolt-Börnstein: Numerical Data and Functional Relationships in Science and Technology*, Vol. 7, Pt. a (Springer-Verlag, Berlin, 1973).

[39] *Landolt-Börnstein: Numerical Data and Functional Relationships in Science and Technology*, Vol. 6 (Springer-Verlag, Berlin, 1971).